Photochemistry and Photobiology, 2013, 89: 1375–1382

# Photoinduced Electron Transfer in Perylene-$TiO_2$ Nanoassemblies†

**Manuel J. Llansola-Portoles[1], Jesse J. Bergkamp[1], John Tomlin[1], Thomas A. Moore[1], Gerdenis Kodis[1], Ana L. Moore*[1], Gonzalo Cosa[2] and Rodrigo E. Palacios*[3]**

[1]Department of Chemistry and Biochemistry, Center for Bioenergy and Photosynthesis, Arizona State University, Tempe, AZ
[2]Department of Chemistry and Center for Self Assembled Chemical Structures (CSACS/CRMAA), McGill University, Montreal, QC, Canada
[3]Departamento de Química, Facultad de Ciencias Exactas Físico-Químicas y Naturales, Universidad Nacional de Río Cuarto, Río Cuarto, Córdoba, Argentina

**Received 2 April 2013, accepted 21 May 2013, DOI: 10.1111/php.12108**

## ABSTRACT

**The photosensitization effect of three perylene dye derivatives on titanium dioxide nanoparticles ($TiO_2$ NPs) has been investigated. The dyes used, *1,7-dibromoperylene-3,4,9,10-tetracarboxy dianhydride* (1), *1,7-dipyrrolidinylperylene-3,4,9,10-tetracarboxy dianhydride* (2) and *1,7-bis(4-tert-butylphenyloxy) perylene-3,4,9,10-tetracarboxy dianhydride* (3) have in common bisanhydride groups that convert into $TiO_2$ binding groups upon hydrolysis. The different substituents on the bay position of the dyes enable tuning of their redox properties to yield significantly different driving forces for photoinduced electron transfer ($P_{eT}$). Recently developed $TiO_2$ NPs having a small average size and a narrow distribution ($4 \pm 1$ nm) are used in this work to prepare the dye-$TiO_2$ systems under study. Whereas successful sensitization was obtained with 1 and 2 as evidenced by steady-state spectral shifts and transient absorption results, no evidence for the attachment of 3 to $TiO_2$ was observed. The comparison of the rates of $P_{eT}$ ($k_{PeT}$) for 1- and 2-$TiO_2$ systems studied in this work with those obtained for previously reported analogous systems, having $TiO_2$ NPs covered by a surfactant layer (Hernandez *et al*. [2012] *J. Phys. Chem. B*., 117, 4568–4581), indicates that $k_{PeT}$ for the former systems is slower than that for the later. These results are interpreted in terms of the different energy values of the conduction band edge in each system.**

## INTRODUCTION

Photoinduced electron transfer ($P_{eT}$) at dye-semiconductor interfaces plays a central role in a number of technological applications such as solar cells (1–4), light-emitting diodes (5,6), field effect transistors (7–9), advanced catalytic processes (10,11), optoelectronic transducers, *etc*. The detailed study of photoinduced processes in functioning devices is in general complicated by the spatial heterogeneity of the organic–inorganic interfaces at the nanoscale. The large number of possible dye to semiconductor binding geometries (including dye binding modes, nanoparticle size and distribution) and the potential for generation of dye aggregates are some of the main factors that contribute to the heterogeneity of these systems and limit the detailed study of $P_{eT}$ processes.

One of the strategies used to try to understand and minimize the heterogeneity effect is to study electron transfer processes in well-defined model nanoassemblies comprised of organic dyes bound to metal oxide particles in suspension (12–21). We recently published a study of $P_{eT}$ processes on a system consisting of perylene dyes bound to $TiO_2$ NPs inside a micellar structure (dye-$TiO_2$@micelle) (22). We selected perylene dyes because they are highly photostable and amenable to the tuning of both their redox and their $TiO_2$ binding properties through chemical functionalization (23–31). To reduce the size distribution of the inorganic nanoparticles in our previous work, we performed the synthesis of $TiO_2$ particles inside the water pool of reverse micelles (which function as a controlled size nano-reactor). However, the presence of surfactant groups surrounding the titanium dioxide nanoparticles ($TiO_2$ NPs) ($TiO_2$@micelles) hindered the binding of some of the dyes due to steric effects and potentially affected the $P_{eT}$ processes in dye-$TiO_2$@micelle nanoassemblies due to the electric field generated by the surfactant polar heads and corresponding counterions.

Herein we report on the study of $P_{eT}$ on dye-$TiO_2$ systems assembled from $TiO_2$ NPs prepared without surfactant molecules and suspended in an organic solvent. Steady-state and transient absorption results indicate that in these systems a significant portion of dyes **1** and **2** can bind to $TiO_2$ NPs and undergo $P_{eT}$ whereas dye **3** is observed to not bind to naked $TiO_2$. The rate constants for charge injection and charge recombination for dye **1**- and dye **2**-$TiO_2$ systems are discussed and compared to those previously acquired with $TiO_2$ NPs prepared within micellar systems. Advantages and disadvantages for both preparations in terms of the dye-nanoparticle assembly and of charge injection and charge recombination rates are discussed.

## MATERIALS AND METHODS

*Materials.* Titanium tetrachloride (≥97.0%) and dichloromethane (anhydrous, 99.5%) were purchased from Sigma-Aldrich and used as received, all other materials for the preparation of compounds **1**, **2** and **3** were the same as reported in reference (22).

*Synthesis.* Perylenes **1** (*1,7-dibromoperylene-3,4,9,10-tetracarboxy dianhydride*), **2** (*1,7-dipyrrolidinylperylene-3,4,9,10-tetracarboxy dianhy-*

*Corresponding author emails: amoore@asu.edu (Ana Moore), rpalacios@exa.unrc.edu.ar (Rodrigo Palacios)
†This article is part of the Special Issue dedicated to the memory of Elsa Abuin.

*dride*) and **3** *1,7-bis(4-tert-butylphenyloxy)perylene-3,4,9,10-tetracarboxy dianhydride* were prepared following literature procedures (22,30,32).

Titanium dioxide nanoparticles of (4 ± 1) nm size (see Figure S1) were prepared by a nonhydrolytic condensation method involving the elimination of alkyl halide between metal alkoxides and metal halides (33–35) (M. J. Llansola-Portoles, unpublished). The resulting $TiO_2$ NPs were dried in ultrahigh vacuum at 25°C for 8 h to remove physisorbed HCl, which was produced in the synthesis, from the surface of the $TiO_2$ NPs. After drying, the resulting NP powder was added to freshly distilled THF to achieve the desired NP concentration. Small amounts of HCl remain present on the surface of the $TiO_2$ NPs (see Supporting Information). Therefore, the NPs zeta potentials kept positive preventing agglomeration and further condensation of the NPs in THF.

Binding of perylenes **1** and **2** to $TiO_2$ NPs was carried out by addition of 100 $\mu$L of a stock solution of the dyes ($\sim 10^{-4}$ M) in THF to 3 mL of a $TiO_2$ NP suspension ($[TiO_2] = 0.1$ g $L^{-1}$) in THF (for pump-probe experiments dye concentration was increased 10 times in an attempt to maximize the amount of dye attached and thus improve the signal corresponding to dye-$TiO_2$ assemblies). The system was left incubating for >12 h and absorption spectra were recorded at periodic time intervals immediately after addition of the dye.

*Instruments and measurements.* Absorption spectra were measured on a Shimadzu UV-3101PC UV-vis-NIR spectrometer. Steady-state fluorescence spectra were measured using a Photon Technology International MP-1 spectrometer, measurements were corrected for the detection system response. Excitation was provided by a 75 W xenon-arc lamp and a single grating monochromator. Fluorescence was collected at 90° to the excitation beam. Fluorescence was detected *via* a single grating monochromator and an R928 photomultiplier tube operating in the single photon counting mode.

Fluorescence decay measurements were performed by the time-correlated single-photon-counting method (TC-SPC). The excitation source was a fiber supercontinuum laser based on a passive modelocked fiber laser and a high-nonlinearity photonic crystal fiber supercontinuum generator (Fianium SC450). The laser provides 6-ps pulses at a repetition rate variable between 0.1 and 40 MHz. The laser output was sent through an Acousto-Optical Tunable Filer (Fianium AOTF) to obtain excitation pulses at desired wavelength. Fluorescence emission was detected at the magic angle using a double grating monochromator (Jobin Yvon Gemini-180) and a microchannel plate photomultiplier tube (Hamamatsu R3809U-50). The instrument response function was 35–55 ps. The spectrometer was controlled by software based on the LabView programming language and data acquisition was done using a single photon counting card (Becker-Hickl, SPC-830). Fluorescence anisotropy decays were obtained by changing the detection polarization of the fluorescence path parallel or perpendicular to the polarization of the excitation light. The anisotropy decays then were calculated according to Eq. (1), where $I_{VV}(t)$ (or $I_{VH}(t)$) is the fluorescence decay when the excitation light is vertically polarized and only the vertically (or horizontally) polarized portion of fluorescence is detected, denoting that the first and second subscripts represent excitation and detection polarization, respectively. The factor $G$ which is equal to the ratio of the sensitivities of the detection system for vertically and horizontally polarized light can be determined either by so-called tail matching of $I_{VV}(t)$ and $I_{VH}(t)$ or by $I_{HV}(t)/I_{HH}(t)$.

$$r(t) = \frac{I_{VV}(t) - GI_{VH}(t)}{I_{VV}(t) + 2GI_{VH}(t)} \quad (1)$$

The femtosecond transient absorption apparatus consisted of a kilohertz pulsed laser source and a pump-probe optical setup. Laser pulses of 100 fs at 800 nm were generated from an amplified, mode-locked Titanium Sapphire kilohertz laser system (Millennia/Tsunami/Spitfire; Spectra Physics). Part of the laser pulse energy was sent through an optical delay line and focused on to a 3 mm sapphire plate to generate a white light continuum for the probe beam. The remainder of the pulse energy was used to pump an optical parametric amplifier (Spectra Physics) to generate excitation pulses, which were selected using a mechanical chopper. The white light generated was then compressed by prism pairs (CVI) before passing through the sample. The polarization of pump beam was set to the magic angle (54.7°) relative to the probe beam and its intensity adjusted using a continuously variable neutral density filter. The white light probe is dispersed by a spectrograph (300 line grating) onto a charge-coupled device camera (DU420; Andor Tech.). The final spectral resolution was about 2.3 nm for over a nearly 300 nm spectral region. The instrument response function was *ca* 150 fs.

The nanosecond–millisecond transient absorption measurements were made with excitation from an optical parametric oscillator driven by the third harmonic of a Nd:YAG laser (Ekspla NT342B). The pulse width was ~4–5 ns, and the repetition rate was 10 Hz. The detection portion of the spectrometer (Proteus) was manufactured by Ultrafast Systems. The instrument response function was *ca* 4.8 ns.

All TC-SPC and transient absorption data were globally analyzed using locally written software (ASUFIT) (36) developed under MATLAB (Mathworks Inc.) environment. The model and procedure for global fitting have been described in detail in reference (22). Decay associated spectra (DAS) obtained from global analysis can have positive or negative amplitudes as a function of wavelength. Positive amplitudes are obtained where absorbance difference signals ($\Delta A$) are: a) positive ($\Delta A>0$) and decreasing (becoming less positive) in time ($\delta(\Delta A)/\delta t<0$) or b) negative ($\Delta A<0$) and increasing (becoming more negative) in time ($\delta(\Delta A)/\delta t<0$). While negative DAS amplitudes occur where $\Delta A$ signals are: a) positive ($\Delta A>0$) and increasing (becoming more positive) in time ($\delta(\Delta A)/\delta t>0$) or b) negative ($\Delta A<0$) and decreasing (becoming less negative) in time ($\delta(\Delta A)/\delta t>0$). These global analysis procedures have been extensively reviewed and random errors associated with the reported lifetimes obtained from fluorescence and transient absorption measurements are typically ≤5%.

Transmission electron microscopy (TEM) were collected using a Philips CM200 TEM at 200 kV/Cs 1.2 mm/PTP Resolution: 0.25 nm/Focused Probe: 0.5 nm/Imaging Modes: TEM/STEM.

*Multivariate curve resolution (MCR).* MCR with alternating least squares (MCR-ALS) procedures were applied using a MATLAB-based routine developed by R. Tauler and A. de Juan. The software is available for free at www.ub.es/gesq/mcr/als2004.htm. Non-negativity (measured and estimated absorbances and concentrations in an experiment will always be nonnegative) and closure (sum of concentrations is forced to be equal to a constant value at each stage) constraints were used to obtain a unique solution. More details on the application of the method and program use can be found in the operating manual at http://www.ub.edu/mcr/als2004/manual.pdf.

## RESULTS AND DISCUSSION

### Dye structure and energetics

The molecular structures of the perylene derivatives used as sensitizers in this work are shown in Scheme 1a. All dyes have two anhydride groups that are subject to hydrolysis under basic conditions (see Scheme 1b) or in the presence of $TiO_2$ NPs to yield

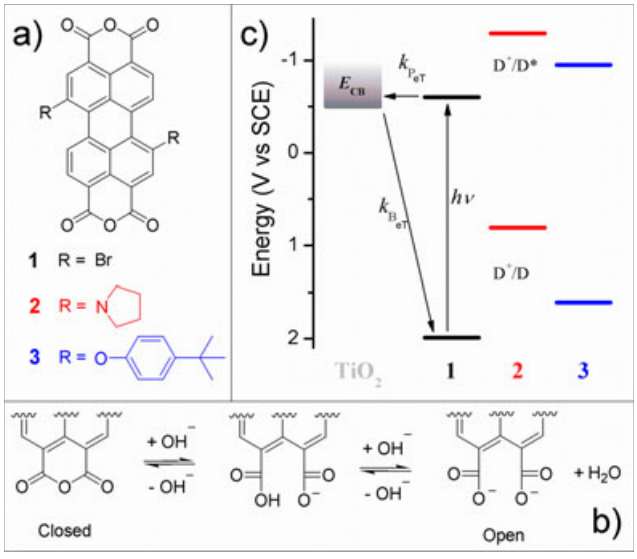


**Scheme 1**

the corresponding dicarboxylate groups (22). In their hydrolyzed "open form," the dyes are able to bind to the surface of $TiO_2$ NPs through the dicarboxylate anchoring group by chemical bonding and/or electrostatic attraction (22,37,38) to yield the open, bound dye species. The redox properties of the dyes were tuned by the attachment of electron donating or withdrawing groups at the bay positions. Scheme 1c shows the energy diagram of the dye-$TiO_2$ system taken from reference (22). In this diagram, the energy for the conduction band edge ($E_{CB}$) of the $TiO_2$ NPs was estimated as the flat band potential ($V_{fb}$) of polycrystalline $TiO_2$ in water at pH = 2 ($V_{fb,W/pH=2} = -0.52$ V, *vs* Standard calomel electrode, SCE) to account for the concentration of protons inside the micelle water pool (where the $TiO_2$ NPs were synthesized) (22,39). On the other hand, the $TiO_2$ NPs used for the experiments described in this work are suspended in a THF solution, which contains trace amounts of acidic water. The $V_{fb}$ of $TiO_2$ in neat THF has been reported as $V_{fb,THF} = -2.34$ V (*vs* SCE) (39). However, the $V_{fb}$ in nonaqueous solutions is mainly determined by the potential establishment of proton adsorption–desorption equilibrium involving solvent molecules and $TiO_2$ (39). As such equilibrium is not possible in nonaqueous aprotic solvents (*e.g.* THF) the $V_{fb}$ value in these solvents is strongly affected by trace amounts of protic impurities (*e.g.* the presence of trace amounts of water leads to significantly positive shifts in $V_{fb}$) (39). Considering these factors, the effective $E_{CB}$ value for the $TiO_2$ NPs used in this study cannot be accurately defined, but it is estimated to fall between $-0.52$ and $-2.34$ V (*vs* SCE). As will be discussed, transient-absorption experiments show evidence for $P_{eT}$ in **1**-$TiO_2$ and **2**-$TiO_2$ systems indicating that the effective $E_{CB}$ in these systems must be only slightly more negative than $-0.52$ V so that $P_{eT}$ from the dyes excited state to the $TiO_2$ CB is thermodynamically favorable.

### Dye-$TiO_2$ nanoassemblies

*Steady-state absorption.* The binding of the dyes to $TiO_2$ NPs was followed by monitoring over time the shift of their absorption spectra in the presence of NPs. This is possible because upon opening of the anhydride ring and binding to $TiO_2$ the absorption spectra of the dyes shift to higher energies (25–27,30,40). This shift can be associated with a reduction in the effective conjugation length of the chromophore (24,25,27,41) and has been previously characterized for the dyes used in this work in ethanolic solution and upon binding of **1** and **2** to $TiO_2$ (22). Figure 1 shows the absorption spectra as a function of time following addition of dye to a $TiO_2$ NP suspension in THF. For the **1**-$TiO_2$ system a significant absorbance shift was observed after 12 h (Fig. 1a) indicating that binding of the dye is slow under the studied conditions. In contrast, significant changes in the absorption occurred within 30 min for the **2**-$TiO_2$ system (Fig. 1b, inset). The magnitude of the absorption shift (~70 nm) observed upon incubation of dye **2** with surfactant-free ("naked") $TiO_2$ NPs (**2-$TiO_2$**) is significantly larger than that previously observed upon incubation with $TiO_2$ NP covered by a layer of surfactant molecules (**2-$TiO_2$**@micelle) (~24 nm) (22). In addition, the absorption shift observed for the **2-$TiO_2$** system is similar to that previously observed upon exhaustive basic hydrolysis of dye **2** in ethanol solution (where presumably both anhydride groups are hydrolyzed yielding a maximum absorption shift of ~130 nm) (22). These observations are consistent with the idea

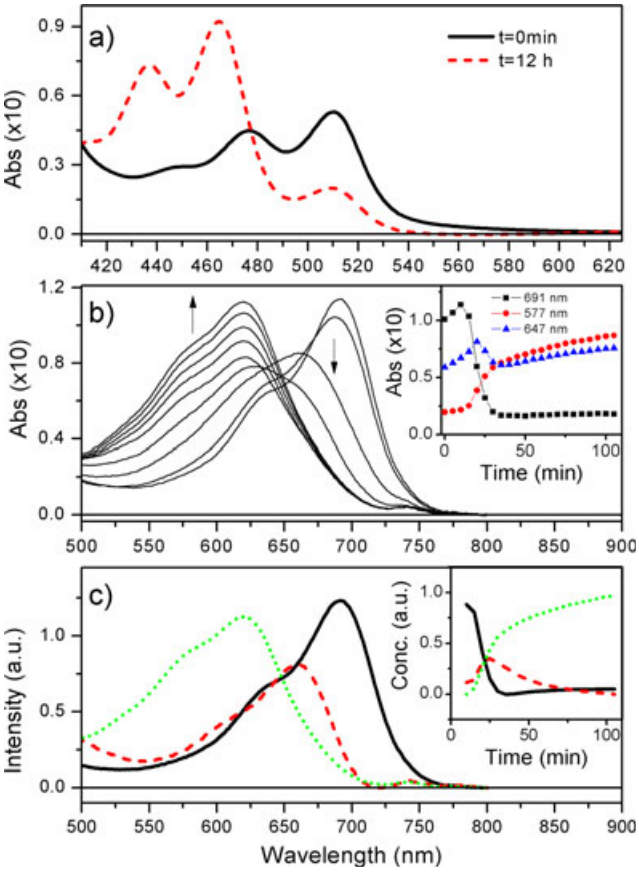


**Figure 1.** (a) Time sequence of absorption spectra collected after addition of **1** to a suspension of titanium dioxide nanoparticles in THF. [Dye] = ~$10^{-6}$ M, estimated [NP] = ~0.1 mg $mL^{-1}$. (b) Same as (a) for dye **2**. The first and last spectra were collected at 0 and 105 min, respectively. The inset displays kinetic traces at specific wavelengths. (c) Species spectra obtained by multivariate curve resolution analysis of data in (b). The inset shows the concentration time evolution for each species (line style coded).

that binding of dye **2** to naked $TiO_2$ NPs can occur at least partly through both dicarboxylic acid groups (product of the hydrolysis of both anhydride rings) whereas dye **2** binds to $TiO_2$@micelle NPs *via* one dicarboxylic acid moiety (resulting from hydrolysis of only one anhydride ring). The surfactant molecules on the $TiO_2$@micelle NPs presumably preclude the formation of dye-NP geometries where both anhydride rings are close enough to the NP surface (and/or remaining water pool) to hydrolyze and bind simultaneously. Thus, dye-NP binding geometries involving both dicarboxylic groups in one particle and others where the dye acts as a bridge between two NPs are in principle possible for naked $TiO_2$ NPs, but very unlikely for $TiO_2$@micelle NPs.

To identify the spectra of the different species present upon hydrolysis and subsequent binding of **2** to $TiO_2$ NPs we used MCR techniques. Analysis of the absorption spectra time sequence shown in Fig. 1b using the MCR-ALS method (42) is shown in Fig. 1c. The results indicate the presence of three species with distinct peak absorptions at 691 nm (Species A), 658 nm (Species B) and 620 nm (Species C) that can be in principle associated with the hydrolysis of none, one and both anhydride rings, respectively. The inset shows the concentration of each species as a function of time indicating a stepwise interconversion between species, *i.e.* A ↔ B ↔ C. The assignment of

A, B and C species to the closed, mono-hydrolyzed and di-hydrolyzed dye species is further supported by MCR analysis of data corresponding to the basic hydrolysis of **2** in ethanol (see Figure S2a), which also shows the presence of three interconverting species (driven by basic titration) with spectral features analogous to the species shown in Fig. 1C. Similar analysis of the data corresponding to the incubation of dye **2** with $TiO_2$@micelle NPs (22) yields only two species with peak absorptions at 688 and 664 nm (see Figure S2b) presumably corresponding to the closed and mono-hydrolyzed species.

In contrast to the spectral shift observed for **1** and **2** in the presence of $TiO_2$ NPs, the absorption spectrum of dye **3** did not significantly shift over time under the same conditions (see Figure S3). This result suggests that dye **3** does not bind to naked $TiO_2$ NPs and thus no additional experiments to investigate $P_{eT}$ were performed with this dye-$TiO_2$ NP system. Further evidence and discussion for the lack of binding of **3** is given in the time-resolved fluorescence anisotropy section (see below).

*Steady-state and time-resolved emission.* Recently we reported a large quenching of dye emission (due to $P_{eT}$) upon binding of **1** and **2** to $TiO_2$ in a micellar system (22). Attempts to quantitatively determine dye emission quenching for **1** and **2** in solution by steady-state fluorescence measurements with and without naked $TiO_2$ NPs failed due to the presence of unattached dyes and of dye aggregates (see time-resolved fluorescence measurements below), which partially dissolve over time and then bind to the $TiO_2$ NPs.

Time-resolved fluorescence measurements (TC-SPC) were performed to investigate the kinetics of the emission of dyes **1** and **2** in the presence of $TiO_2$ NPs (see Figure S4a and b, respectively). Results for solutions of **1** incubated with $TiO_2$ NPs show fluorescence decay-associated spectra (DAS) with three components of 100 ps, 850 ps and 3.9 ns ($\chi^2 = 1.18$). The 100 and 850 ps components could be associated with dye aggregates where the dye is in the closed form suspended in solution and showing significant autoquenching. It is well known that perylenes are prone to aggregate and crystallize to afford typically weakly luminescent particles (43,44). The main driving force for aggregation comes from strong intermolecular $\pi-\pi$-stacking interactions resulting from the extended $\pi$-system and large quadrupole moment of perylenes. The most likely fluorescence quenching mechanisms in these putative aggregates are: (1) enhancement in the rate of internal conversion to the ground state due to increased coupling of electronic excitation to lattice vibrations, (2) exciton (dipole–dipole) interactions and (3) efficient energy transfer to nonemitting defects or impurities (45,46). Alternatively, the 100 and 850 ps components could be associated with the emission of the dye when physisorbed on the surface of NPs in its closed form and thus with a low electronic coupling for $P_{eT}$. The 3.9 ns component is associated with the emission from **1** in its closed form and nonaggregated in solution. On the other hand, the fluorescence DAS of solutions of **2** incubated with $TiO_2$ NPs yielded two fluorescence DAS components ($\chi^2 = 1.12$) with lifetime of 71 ps and 2.5 ns. The 71 ps component with maximum at 740 nm could be associated with aggregates of **2** closed species, which show a short fluorescence lifetime due to autoquenching. The 2.5 ns component is associated with **2** in its closed form and nonaggregated in solution.

*Time-resolved fluorescence anisotropy.* To further investigate the diffusion rotational properties of the emitting species in the studied samples we performed time-resolved fluorescence anisotropy measurements. Figure 2 shows time-resolved fluorescence anisotropy decays of the dyes in THF solutions with and without the addition of $TiO_2$ NPs. As seen in Fig. 2a, the decay of dye **1** in solution can be fitted with a single exponential lifetime of 115 ps similar to that observed in n-heptane (81 ps) (22). In the presence of $TiO_2$ NPs, the anisotropy decay can only be satisfactorily fitted with two exponential components (115 and 890 ps). The shorter component can be associated with the reorientation dynamics of free dye in solution or energy transfer among dyes in aggregates since both situations are possible and create a fast depolarization effect in the emission. The 890 ps component can be ascribed to the presence of dye molecules physisorbed on the surface of $TiO_2$ NPs or covalently bound to surface defects such that the effective dye-$TiO_2$ electronic coupling (H) for $P_{eT}$ is very small and consequently the dye fluorescence is not significantly quenched. These putative dye-$TiO_2$ assemblies are significantly larger than a free dye in solution and consequently have much slower reorientation dynamics. To test this, we calculated the radius of a sphere with an 890 ps rotational correlation time in THF (see Supporting Information); the obtained value, $r = 1.2$ nm, is in close agreement with the size of our $TiO_2$ NPs (diameter $4 \pm 1$ nm). An analogous situation, but with longer time constants, is observed for dye **2** (see

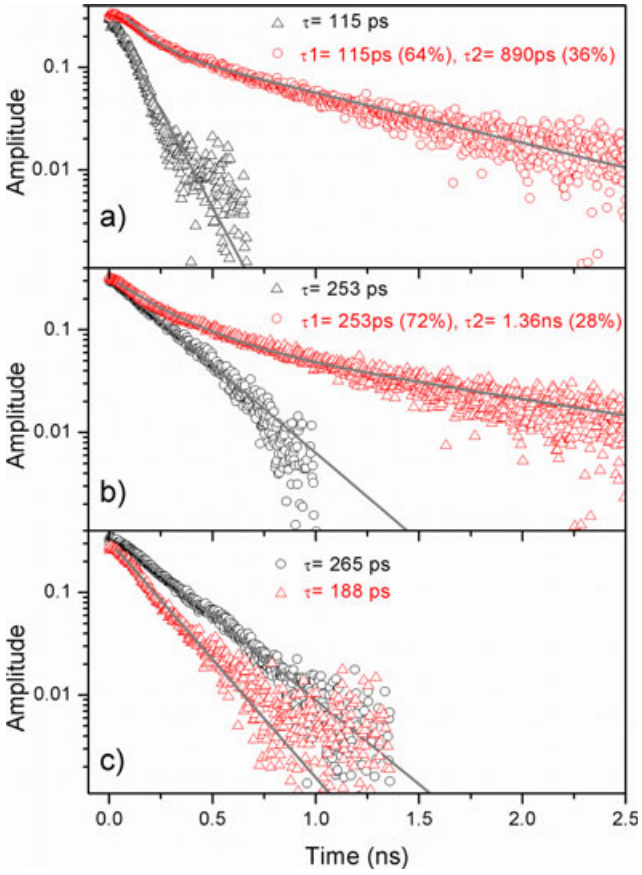


**Figure 2.** (a) Fluorescence anisotropy decays (data points) of **1** in THF without (circles) and with titanium dioxide nanoparticles (triangles). Smooth lines show exponential fits to the data. Samples were excited and emission collected at the following wavelengths: $\lambda_{ex} = 450$ nm $\lambda_{em} = 550$ nm. (b) Same as (a) for dye **2**: $\lambda_{ex} = 600$ nm $\lambda_{em} = 760$ nm. (c) Same as (a) for dye **3**: $\lambda_{ex} = 450$ nm and $\lambda_{em} = 550$ nm. Dye concentration was $\sim 10^{-6}$ M for all samples.

Fig. 2b). The free dye in solution shows a mono-exponential decay with a lifetime of 253 ps and in the presence of NPs it shows a bi-exponential decay with 253 ps and 1.36 ns components. These results are consistent with the larger molecular size of **2** *vs* **1** (22) and consequently slower reorientation. In contrast to this, dye **3** shows fast mono-exponential decays for both situations, the free dye in solution (265 ps) and in the presence of $TiO_2$ NPs (188 ps) (see Fig. 2c). The results indicate that dye **3** does not exhibit physisorption or bind to $TiO_2$ NPs which is consistent with the lack of absorption shift observed when the dye is incubated in the presence of NPs (see Figure S3). The lack of binding of dye **3** to $TiO_2$@micelles NPs was previously reported by our group and rationalized invoking strong steric interactions between surfactant molecules and the bulky t-butylphenoxy groups of the dye which prevented the formation of geometries where one anhydride ring was close enough to the $TiO_2$ surface to achieve binding (22). The new results presented herein indicate that even in absence of micelles in the system, the t-butylphenoxy groups present strong steric hindrance to reach dye-$TiO_2$ NPs geometries necessary for efficient attachment.

*Time-resolved absorption.* Time-resolved transient absorption techniques were used to investigate the kinetics of $P_{eT}$ in the dye-$TiO_2$ nanoassemblies. Measurements in the femtosecond to nanosecond (pump-probe) and nanosecond to microsecond (flash-photolysis) time ranges were performed in an attempt to measure the kinetics of formation and recombination, respectively, of the **dye**$^{\bullet+}$-$TiO_2(e^-)$ charge separated state.

Figure 3a and c shows pump-probe results for the **1**-$TiO_2$ system with excitation at 490 nm. Global analysis of the kinetic data shows four decay components with lifetimes of ~500 fs, 2.3 ps, 45 ps, and 2.7 ns (see Fig. 3a). The DAS of the 500 fs component can be attributed to $P_{eT}$ from **1** open, bound species to $TiO_2$ to form the **1**$^{\bullet+}$-$TiO_2(e^-)$ state. The following spectral features support this assignment: (1) decay of stimulated emission (negative amplitude) corresponding to **1** open, bound at ~520 nm (see Figure S5a, red dashed line), (2) formation of **1** radical cation (negative amplitude) with characteristic induced absorption at ~630 nm and (3) formation of free carriers (injected electrons) in the $TiO_2$ semiconductor ($TiO_2(e^-)$) (negative amplitude) with absorption around 1000 nm. The 2.3 and 45 ps components show a mixture of two main processes: (1) decay of singlet excited state of the **1** closed species (as seen in the TC-SPC data, Figure S4a) and (2) decay of the **1**$^{\bullet+}$-$TiO_2(e^-)$ charge separated state with positive amplitudes at ~630 nm (**1**$^{\bullet+}$ absorption) and 850−1000 nm ($TiO_2(e^-)$ absorption). The last 2.7 ns DAS can be attributed mostly to the decay of singlet excited state of **1** closed form (presumably free in solution), showing ground state bleaching and stimulated emission from ~520 to 570 nm, and induced absorption at 470 and 750 nm.

Transient absorption measurements on the **1**-$TiO_2$ system in the nanosecond to millisecond time range were performed to complement the pump−probe data; the results are shown in Fig. 3b. Global analysis of the kinetics in argon-saturated solution yields two components, 2.5 ms and 12 $\mu$s (excitation at 440 nm). The 2.5 ms component is associated with the decay of the **1**$^{\bullet+}$-$TiO_2(e^-)$ state showing positive amplitude signals around 630 nm (**1**$^{\bullet+}$ absorption, see kinetic trace in Fig. 3b inset) and up to ~950 nm ($TiO_2(e^-)$). The 12 $\mu$s component is oxygen sensitive and it is associated with the decay of triplet excited states of **1** (in open and closed forms) showing transient absorption in the ~500–700 nm range and ground state bleaching at 450 and 520 nm (small dip).

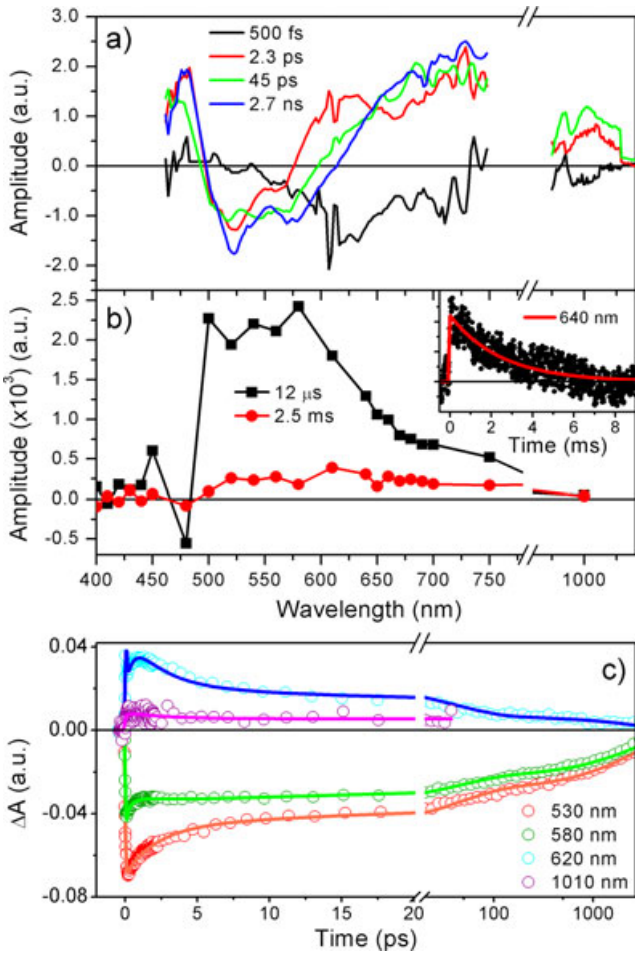


**Figure 3.** (a) Decay associated spectra of **1**-$TiO_2$ nano-assemblies in THF solution measured by pump-probe (fs to ns range). Data were acquired with pump laser excitation at $\lambda_{ex}$ = 490 nm. (b) Same as (a) measured by flash-photolysis (ns to $\mu$s range) upon $\lambda_{ex}$ = 440 nm. (c) Kinetics traces (data points) and fits (smooth lines) at selected wavelengths corresponding to the data shown in (a).

Figure 4a and c show pump-probe results with excitation at 650 nm for **2**-$TiO_2$ nanoassemblies. Global fit to the data yields four DAS components of 260 fs, 3.4 ps, 130 ps and 1.9 ns (see Fig. 4a). The 260 fs component is mainly associated with singlet energy transfer from the open form of the dye to the closed one and possibly, to some extent, to the formation of the **2**$^{\bullet+}$-$TiO_2(e^-)$ charge separated state. This component shows the following spectral features: (1) stimulated emission decay (negative amplitude) of **2** open species in the 660–730 nm region (consistent with the red dashed spectra in Figure S5b), (2) formation of stimulated emission of the dye in its closed form with a positive amplitude around 760 nm and (3) **2**$^{\bullet+}$ transient absorption formation (negative amplitude) above 650 nm. In addition to this, the ground state bleaching of open dye **2** (around 600 nm) decays to some extent with the same lifetime (260 fs) and there is no rise with 260 fs at 1000 nm. Therefore, we do not have strong spectral evidence of **2**$^{\bullet+}$-$TiO_2(e^-)$ formation on the time scales measured. It is likely that charge separation is very fast and occurs in less than 150 fs (instrument response time of our apparatus). Transient absorption at 1015 nm supports this assumption showing a kinetic trace with

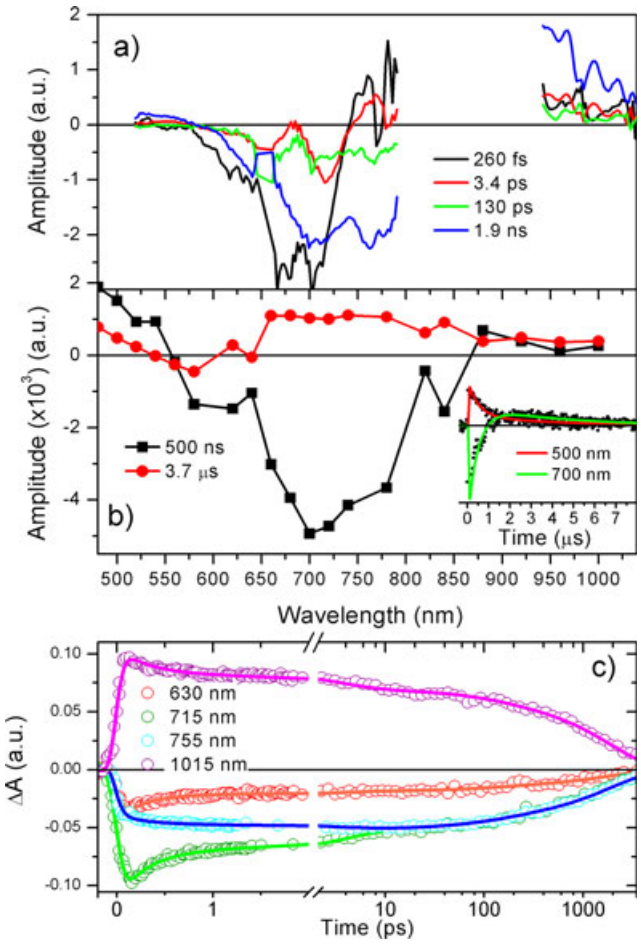


**Figure 4.** (a) Decay associated spectra of **2**-$TiO_2$ nano-assemblies in THF solution measured by pump-probe (fs to ns range). Data were acquired with pump laser excitation at $\lambda_{ex}$ = 650 nm. (b) Same as (a) measured by flash-photolysis (ns to $\mu$s range). $\lambda_{ex}$ = 640 nm. (c) Kinetic traces (data points) and fits (smooth line) at selected wavelengths corresponding to the data shown in (a).

instantaneous rise, limited by instrument response (see Fig. 4c, violet data points). The 3.4 ps DAS component is assigned to solvation-induced band-shift of the emission band of **2** closed species. The 130 ps and 1.9 ns components show a mixture of two main processes: (1) recovery of ground state bleaching and stimulated emission of **2** closed species (presumably slightly aggregated and/or physisorbed on the NPs) consistent with its close temporal match to the emission DAS components shown in Figure S4b (71 ps and 2.5 ns) and (2) recovery of ground state bleaching of the open-bound form of **2** (due to recombination of the **2**$^{\bullet+}$-$TiO_2(e^-)$ state) showing negative amplitude in the region around 640 nm.

Figure 4b shows flash-photolysis results with excitation at 640 nm for the **2**-$TiO_2$ system. Global analysis of the data yields two DAS components of ~500 ns and 3.7 $\mu$s. The shorter component is associated with the triplet state of the dye in its closed and open forms showing ground state absorption bleaching recovery (negative amplitude) from 570 to ~800 nm (**2** closed species, see Fig. 4a, solid black spectrum) and triplet state transient absorption decay (positive amplitude) below 550 nm. The 3.7 $\mu$s component is associated with the decay of the **2**$^{\bullet+}$-$TiO_2(e^-)$ charge separated state. This long component shows ground state bleaching of **2** fully open bound species in the 500–650 nm region (consistent with the solid red spectra, Figure S5b) and **2**$^{\bullet+}$ transient absorption above 650 nm (consistent with previously reported transient features of **2**$^{\bullet+}$ [22]).

A comparison of the dynamics of $P_{eT}$ in dye-$TiO_2$@micelle NPs *vs* dye-$TiO_2$ systems shows that the $P_{eT}$ rate ($k_{PeT}$ Scheme 1c) for **1**-$TiO_2$ ($k_{PeT}$ [**1**, naked] = 1/500 fs) is slower than that for **1**-$TiO_2$@micelle ($k_{PeT}$ [**1**, micelle] = 1/210 fs). On the other hand, for both the **2**-$TiO_2$@micelle and **2**-$TiO_2$ systems, the corresponding $k_{PeT}$ rates are faster than the time resolution of our pump-probe instrument, so no comparison can be made in this case. Regarding the kinetics of recombination of the **dye**$^{\bullet+}$-$TiO_2(e^-)$ state ($k_{BeT}$, Scheme 1c), $k_{BeT}$ (**1**, naked) = 1/2.5 ms is slower than $k_{BeT}$ (**1**, micelle) ~1/1.5 ms and $k_{BeT}$ (**2**, naked) = 1/3.7 $\mu$s is faster than $k_{BeT}$ (**2**, micelle) ~1/30 ms.

The measured $P_{eT}$ rate constants can be discussed in terms of Eq. (2) (12,47–51), where $\rho$ ($E$) is the effective density of states at the energy $E$ relative to the conduction band edge ($E_{CB}$), $f(E)$ represents the Fermi distribution function, $\bar{H}(E)$ is the average electronic coupling between the dye excited state and all $k$ states in the semiconductor, $\lambda$ is the total reorganization energy, and $\Delta G^0 = E_{CB} - E(D^+/D^*)$. To a first approximation $\bar{H}(E)$ and $\lambda$ are assumed to be the same for all the dye-$TiO_2$ systems given the analogous structure of the dyes and their expected identical binding modes to the $TiO_2$ surface.

$$k_{PeT} = \frac{2\pi}{\hbar}\int_{-\infty}^{\infty}\rho(E)(1-f(E))|H(E)|^2(4\pi\lambda k_B T)^{-1/2}e^{-\frac{(\lambda+\Delta G^0+E)^2}{4\lambda k_B T}}dE \quad (2)$$

As was discussed before, the $E_{CB}$ (naked) is more negative than $E_{CB}$ (micelle), thus $|\Delta G^0(\text{naked})| < |\Delta G^0(\text{micelle})|$ and $k_{PeT}(\text{naked}) < k_{PeT}(\text{micelle})$ (assuming $P_{eT}$ in the normal Marcus region [52]), which is consistent with the experimental results.

Since models for $k_{BeT}$ involve charge trapping and transport effects which are not well defined in our NPs no detailed analysis is presented for this case.

## CONCLUSIONS

The main objective of this work was to study the sensitization effect of perylene dyes in surfactant-free $TiO_2$ NPs with small average size and relatively narrow size distribution in THF. In principle, these particles present the opportunity to construct simple dye-$TiO_2$ systems, as compared to the previously reported dye-$TiO_2$@micelle assemblies, to investigate $P_{eT}$ processes. The added surfactant layer in the later systems presumably affects the dye-$TiO_2$ $P_{eT}$ processes due to the highly directional electric field produced by the surfactant polar groups and corresponding counterions. Thus, in this sense the dye-$TiO_2$@micelle systems are complex ones characterized by a larger number of variables as compared to the dye-$TiO_2$ systems used in this study. However, problems related to dye aggregation in THF and the potential formation of dye-NP aggregates in which two NPs can be linked by bridging perylenes (due to its ability to function as bifunctional anchors) created unanticipated complications in the formation of the dye-$TiO_2$ systems studied herein. In the case of bridging, the micelle structure provides an organizing scaffold that prevents the formation of NPs aggregates. The results of this study highlight the importance of several factors including solubility, the presence of multiple

anchoring groups and steric hindrance of bay groups that affect binding geometries that must be considered in the design of perylene derivative dyes as $P_{eT}$ sensitizers for inorganic semiconductor NPs.

*Acknowledgements*—This work has been supported in part by the National Science Foundation, USA, DMR-0908656 (synthetic studies) and as part of the Center for Bio-Inspired Solar Fuel Production, an Energy Frontier Research Center funded by the U.S. Department of Energy, Office of Science, Office of Basic Energy Sciences under Award Number DE-SC0001016 (transient spectroscopic studies). Additional support was given by grants from the following: the Agencia Nacional de Promoción Científica y Tecnológica (ANPCyT), Argentina (PICT 140/08, 2213/07, 2691/11 and PRH23 PME01); the Consejo Nacional de Investigaciones Científicas y Técnicas (CONICET), Argentina (PIP 11220090100839/10, 11220100100284/11 and CIAM/09); the Secretaría de Ciencia y Técnica, UNRC Argentina; the Ministerio de Ciencia y Tecnología Cordoba, Argentina (PID 033/2010). We also thank funding from the National Science and Engineering Research Council (Canada) and a Tomlinson Award, McGill University. R.E.P. is permanent research staff of CONICET.

## SUPPORTING INFORMATION

Additional Supporting Information may be found in the online version of this article:

**Figure S1**. TEM micrographs of $TiO_2$ NPs.

**Figure S2**. (a) Species spectra obtained by MCR analysis of **2** in ethanol solution with and without addition of KOH and $TiO_2$ NPs inside reverse micelles.

**Figure S3**. Time sequence of absorption spectra collected after addition of **3** to a suspension of **$TiO_2$** NPs in THF.

**Figure S4.** Fluorescence decay associated spectra of Dyes **1** and 2 in THF.

**Figure S5.** (a) Normalized absorption and emission spectra of dyes **1** and 2 in THF before and after the attachment to the $TiO_2$ NP.

**Figure S6.** Transient absorption kinetics traces at selected wavelengths for the **1**-$TiO_2$ and **2**-$TiO_2$ systems in THF.

## REFERENCES

1. Gratzel, M. (2003) Dye-sensitized solar cells. *J. Photochem. Photobiol. C Photochem. Rev.* **4**, 145–153.
2. Gratzel, M. (2009) Recent advances in sensitized mesoscopic solar cells. *Acc. Chem. Res.* **42**, 1788–1798.
3. Hagfeldt, A., G. Boschloo, L. C. Sun, L. Kloo and H. Pettersson (2010) Dye-sensitized solar cells. *Chem. Rev.* **110**, 6595–6663.
4. Hagfeldt, A. and M. Gratzel (2000) Molecular photovoltaics. *Acc. Chem. Res.* **33**, 269–277.
5. Anikeeva, P. O., C. F. Madigan, J. E. Halpert, M. G. Bawendi and V. Bulovic (2008) Electronic and excitonic processes in light-emitting devices based on organic materials and colloidal quantum dots. *Phys. Rev. B Condens. Matter* **78**, 085434.
6. Zhu, X. Y. (2004) Electronic structure and electron dynamics at molecule-metal interfaces: Implications for molecule-based electronics. *Surf. Sci. Rep.* **56**, 1–83.
7. Lindstrom, C. D. and X. Y. Zhu (2006) Photoinduced electron transfer at molecule-metal interfaces. *Chem. Rev.* **106**, 4281–4300.
8. Zhu, X. Y. (2004) Charge transport at metal-molecule interfaces: A spectroscopic view. *J. Phys. Chem. B* **108**, 8778–8793.
9. Coropceanu, V., J. Cornil, D. A. da Silva, Y. Olivier, R. Silbey and J. L. Bredas (2007) Charge transport in organic semiconductors. *Chem. Rev.* **107**, 926–952.
10. Tulevski, G. S., M. B. Myers, M. S. Hybertsen, M. L. Steigerwald and C. Nuckolls (2005) Formation of catalytic metal-molecule contacts. *Science* **309**, 591–594.
11. Kamat, P. V. (1994) Interfacial charge transfer processes in colloidal semiconductor systems. *Prog. React. Kinet.* **19**, 277–316.
12. Anderson, N. A. and T. Q. Lian (2005) Ultrafast electron transfer at the molecule-semiconductor nanoparticle interface. *Annu. Rev. Phys. Chem.* **56**, 491–519.
13. Stipkala, J. M., F. N. Castellano, T. A. Heimer, C. A. Kelly, K. J. T. Livi and G. J. Meyer (1997) Light-induced charge separation at sensitized sol–gel processed semiconductors. *Chem. Mater.* **9**, 2341–2353.
14. Zhang, J. Z. (2000) Interfacial charge carrier dynamics of colloidal semiconductor nanoparticles. *J. Phys. Chem. B* **104**, 7239–7253.
15. Zhang, Y. Y. and E. Galoppini (2010) Organic polyaromatic hydrocarbons as sensitizing model dyes for semiconductor nanoparticles. *ChemSusChem* **3**, 410–428.
16. Hilgendorff, M. and V. Sundström (1998) Dynamics of electron injection and recombination of dye-sensitized $TiO_2$ particles. *J. Phys. Chem. B* **102**, 10505–10514.
17. He, J., J. Zhao, T. Shen, H. Hidaka and N. Serpone (1997) Photosensitization of colloidal titania particles by electron injection from an excited organic dye–antennae function. *J. Phys. Chem. B* **101**, 9027–9034.
18. Joselevich, E. and I. Willner (1994) Photosensitization of quantum-size $TiO_2$ particles in water-in-oil microemulsions. *J. Phys. Chem.* **98**, 7628–7635.
19. Moser, J. and M. Graetzel (1984) Photosensitized electron injection in colloidal semiconductors. *J. Am. Chem. Soc.* **106**, 6557–6564.
20. Sant, P. A. and P. V. Kamat (2002) Interparticle electron transfer between size-quantized CdS and $TiO_2$ semiconductor nanoclusters. *Phys. Chem. Chem. Phys.* **4**, 198–203.
21. Zhang, H., Y. Zhou, M. Zhang, T. Shen, J. Xiang and J. Feng (2003) Nanosecond time-resolved studies of long-lived photoinduced charge separation in the dyad fluorescein–anthraquinone–methyl ester adsorbed on $TiO_2$ colloids. *J. Colloid Interface Sci.* **263**, 669–673.
22. Hernández, L. I., R. Godin, J. J. Bergkamp, M. J. Llansola Portolés, B. D. Sherman, J. Tomlin, G. Kodis, D. D. Méndez-Hernández, S. Bertolotti, C. A. Chesta, E. Mariño-Ochoa, A. L. Moore, T. A. Moore, G. Cosa and R. E. Palacios (2012) Spectral characteristics and photosensitization of $TiO_2$ nanoparticles in reverse micelles by perylenes. *J. Phys. Chem. B* **117**, 4568–4581.
23. Avlasevich, Y., C. Li and K. Mullen (2010) Synthesis and applications of core-enlarged perylene dyes. *J. Mater. Chem.* **20**, 3814–3826.
24. Cappel, U. B., M. H. Karlsson, N. G. Pschirer, F. Eickemeyer, J. Schoneboom, P. Erk, G. Boschloo and A. Hagfeldt (2009) A broadly absorbing perylene dye for solid-state dye-sensitized solar cells. *J. Phys. Chem. C* **113**, 14595–14597.
25. Edvinsson, T., C. Li, N. Pschirer, J. Schöneboom, F. Eickemeyer, R. Sens, G. Boschloo, A. Herrmann, K. Müllen and A. Hagfeldt (2007) Intramolecular charge-transfer tuning of perylenes: Spectroscopic features and performance in dye-sensitized solar cells. *J. Phys. Chem. C* **111**, 15137–15140.
26. Fortage, J., M. Séverac, C. Houarner-Rassin, Y. Pellegrin, E. Blart and F. Odobel (2008) Synthesis of new perylene imide dyes and their photovoltaic performances in nanocrystalline $TiO_2$ dye-sensitized solar cells. *J. Photochem. Photobiol. A* **197**, 156–169.
27. Li, C., J.-H. Yum, S.-J. Moon, A. Herrmann, F. Eickemeyer, N. G. Pschirer, P. Erk, J. Schöneboom, K. Müllen, M. Grätzel and M. K. Nazeeruddin (2008) An improved perylene sensitizer for solar cell applications. *ChemSusChem* **1**, 615–618.
28. Mathew, S. and H. Imahori (2011) Tunable, strongly-donating perylene photosensitizers for dye-sensitized solar cells. *J. Mater. Chem.* **21**, 7166–7174.
29. Planells, M., F. J. Cespedes-Guirao, A. Forneli, A. Sastre-Santos, F. Fernandez-Lazaro and E. Palomares (2008) Interfacial photo-induced charge transfer reactions in perylene imide dye sensitised solar cells. *J. Mater. Chem.* **18**, 5802–5808.
30. Shibano, Y., T. Umeyama, Y. Matano and H. Imahori (2007) Electron-donating perylene tetracarboxylic acids for dye-sensitized solar cells. *Org. Lett.* **9**, 1971–1974.
31. Shibano, Y., H. Imahori and C. Adachi (2009) Organic thin-film solar cells using electron-donating perylene tetracarboxylic acid derivatives. *J. Phys. Chem. C* **113**, 15454–15466.
32. Kohl, C., T. Weil, J. Q. Qu and K. Mullen (2004) Towards highly fluorescent and water-soluble perylene dyes. *Chem. Eur. J.* **10**, 5297–5310.

33. Mutin, P. H. and A. Vioux (2009) Nonhydrolytic processing of oxide-based materials: Simple routes to control homogeneity, morphology, and nanostructure. *Chem. Mater.* **21**, 582–596.
34. Arnal, P., R. J. P. Corriu, D. Leclercq, P. H. Mutin and A. Vioux (1997) A solution chemistry study of nonhydrolytic sol–gel routes to titania. *Chem. Mater.* **9**, 694–698.
35. Vioux, A. (1997) Nonhydrolytic sol–gel routes to oxides. *Chem. Mater.* **9**, 2292–2299.
36. Time-resolved absorption and emission global-analysis software. Available at: http://www.public.asu.edu/~laserweb/asufit/asufit.html. Accessed on 1 June 2013.
37. Nilsing, M., P. Persson, S. Lunell and L. Ojamae (2007) Dye-sensitization of the $TiO_2$ rutile (110) surface by perylene dyes: Quantum-chemical periodic B3LYP computations. *J. Phys. Chem. C* **111**, 12116–12123.
38. Weng, Y.-X., L. Li, Y. Liu, L. Wang and G.-Z. Yang (2003) Surface-binding forms of carboxylic groups on nanoparticulate $TiO_2$ surface studied by the interface-sensitive transient triplet-state molecular probe. *J. Phys. Chem. B* **107**, 4356–4363.
39. Redmond, G. and D. Fitzmaurice (1993) Spectroscopic determination of flatband potentials for polycrystalline titania electrodes in nonaqueous solvents. *J. Phys. Chem.* **97**, 1426–1430.
40. Ferrere, S. and B. A. Gregg (2002) New perylenes for dye sensitization of $TiO_2$. *New J. Chem.* **26**, 1155–1160.
41. Li, C., Z. Liu, J. Schoneboom, F. Eickemeyer, N. G. Pschirer, P. Erk, A. Herrmann and K. Mullen (2009) Perylenes as sensitizers in hybrid solar cells: How molecular size influences performance. *J. Mater. Chem.* **19**, 5405–5415.
42. Multivariate curve resolution software mcr-als gui. Available at: http://www.ub.edu/mcr/web_mcr/download.html. Accessed on 1 June 2013.
43. Würthner, F. (2006) Bay-substituted perylene bisimides: Twisted fluorophores for supramolecular chemistry. *Pure Appl. Chem.* **78**, 2341–2349.
44. Wurthner, F. (2004) Perylene bisimide dyes as versatile building blocks for functional supramolecular architectures. *Chem. Commun.* 1564–1579.
45. Birks, J. B. (1970) *Photophysics of Aromatic Molecules*. John Wiley & Sons Ltd, London.
46. Langhals, H., S. Demmig and T. Potrawa (1991) The relation between packing effects and solid state fluorescence of dyes. *Journal für Praktische Chemie* **333**, 733–748.
47. Sakata, T., K. Hashimoto and M. Hiramoto (1990) New aspects of electron-transfer on semiconductor surface – dye-sensitization system. *J. Phys. Chem.* **94**, 3040–3045.
48. Stockwell, D., Y. Yang, J. Huang, C. Anfuso, Z. Q. Huang and T. Q. Lian (2010) Comparison of electron-transfer dynamics from coumarin 343 to $TiO_2$, $SnO_2$, and ZnO nanocrystalline thin films: Role of interface-bound charge-separated pairs. *J. Phys. Chem. C* **114**, 6560–6566.
49. Gao, Y. Q., Y. Georgievskii and R. A. Marcus (2000) On the theory of electron transfer reactions at semiconductor electrode/liquid interfaces. *J. Chem. Phys.* **112**, 3358–3369.
50. Ai, X., N. A. Anderson, J. C. Guo and T. Q. Lian (2005) Electron injection dynamics of Ru polypyridyl complexes on $SnO_2$ nanocrystalline thin films. *J. Phys. Chem. B* **109**, 7088–7094.
51. Ai, X., J. C. Guo, N. A. Anderson and T. Q. Lian (2004) Ultrafast electron transfer from Ru polypyridyl complexes to $Nb_2O_5$ nanoporous thin films. *J. Phys. Chem. B* **108**, 12795–12803.
52. Kuciauskas, D., M. S. Freund, H. B. Gray, J. R. Winkler and N. S. Lewis (2001) Electron transfer dynamics in nanocrystalline titanium dioxide solar cells sensitized with ruthenium or osmium polypyridyl complexes. *J. Phys. Chem. B* **105**, 392–403.